

PSFC/JA-08-4

## **Monoenergetic Proton Radiography Measurements of Implosion Dynamics in Direct-Drive Inertial Confinement Fusion**

**C. K. Li, F. H. Séguin, J. R. Rygg, J. A. Frenje, M. Manuel, R. D. Petrasso**

*Plasma Science and Fusion Center, Massachusetts Institute of Technology,  
Cambridge, Massachusetts 02139, USA*

**R. Betti<sup>1</sup>, J. Delettrez, J. P. Knauer, F. Marshall, D. D. Meyerhofer<sup>1</sup>,  
D. Shvarts<sup>2</sup>, V. A. Smalyuk, and C. Stoeckl**

*Laboratory for Laser Energetics, University of Rochester, Rochester, New York 14623, USA*

<sup>1</sup>also *Department of Mechanics Engineering, Physics and Astronomy, University of  
Rochester, Rochester, New York 14623, USA*

<sup>2</sup>also *NRCN, Negev and Ben Gurion University of the Negev, Beer-Sheva 84015, Israel*

**O. L. Landen and R. P. J. Town**

*Lawrence Livermore National Laboratory, Livermore, California 94550 USA*

**C. A. Back and J. D.ilkenny**

*General Atomics, San Diego, California, 92186 USA*

1 May 2008

Plasma Science and Fusion Center  
Massachusetts Institute of Technology  
Cambridge, MA 02139 USA

The work described here was performed in part at the LLE National Laser User's Facility (NLUF), and was supported in part by US DOE (Grant No. DE-FG03-03SF22691), LLNL (subcontract Grant No. B504974), and LLE (subcontract Grant No. 412160-001G).

Accepted for publication in *Physical Review Letters*

# Monoenergetic Proton Radiography Measurements of Implosion Dynamics in Direct-Drive Inertial Confinement Fusion

C. K. Li, F. H. Séguin, J. R. Rygg, J. A. Frenje, M. Manuel, and R. D. Petrasso

*Plasma Science and Fusion Center, Massachusetts Institute of Technology, Cambridge, Massachusetts 02139, USA*

R. Betti<sup>1</sup>, J. Delettrez, J. P. Knauer, F. Marshall, D. D. Meyerhofer<sup>1</sup>, D. Shvarts<sup>2</sup>, V. A. Smalyuk, and C. Stoeckl  
*Laboratory for Laser Energetics, University of Rochester, Rochester, New York 14623, USA*

<sup>1</sup>also *Department of Mechanics Engineering, Physics and Astronomy, University of Rochester, Rochester, New York 14623, USA*

<sup>2</sup>also *NRCN, Negev and Ben Gurion University of the Negev, Beer-Sheva 84015, Israel*

O. L. Landen and R. P. J. Town

*Lawrence Livermore National Laboratory, Livermore, California 94550 USA*

C. A. Back and J. D. Kilkenny

*General Atomics, San Diego, California, 92186 USA*

Time-gated, monoenergetic radiography with 15.1-MeV protons provides unique measurements of spherical target implosion dynamics in direct-drive inertial confinement fusion (ICF). Radiographs obtained at different implosion times, from acceleration, through coasting, deceleration, to final stagnation, display a comprehensive picture of spherical ICF implosion. Critical information inferred from such images, hitherto unavailable from conventional measurements, characterizes the spatial structure and temporal evolution of self-generated fields and plasma areal density. Most importantly, the results shown here include the first observation of a radial electric field inside the imploding capsule. It is initially directed inward (at  $\sim 10^9$  V/m), eventually reverses direction ( $\sim 10^8$  V/m), and is the probable consequence of the evolution of the electron pressure gradient.

PACS numbers: 52.57. -z, 52.35. Tc, 52.25. Tx, 52.70. Nc

The goal of inertial confinement fusion (ICF) is ignition and high gain [1], which require that a cryogenic deuterium-tritium (DT) spherical capsule be symmetrically imploded. This implosion results in a small mass of low density, hot fuel at the center, surrounded by a larger mass of high density, low temperature fuel [1]. Shock coalescence ignites the hot spot, and a self-sustaining burn wave subsequently propagates into the main fuel region. In the direct-drive approach to ICF, such an implosion occurs in response to a large number of high-power, individual laser beams illuminating the surface of a capsule. Understanding and controlling implosion dynamics is essential for ensuring success [1].

Implosion dynamics have been studied experimentally with a number of diagnostics, including x-ray imaging [1-3], fusion-product spectrometry [4], and fusion product imaging [5,6], but none of these provide a complete picture of the time evolution of mass assembly and self-generated electric ( $E$ ) and magnetic ( $B$ ) fields.

In this Letter we present new nuclear observations of implosion dynamics for direct-drive spherical capsules on the OMEGA laser facility [7], using monoenergetic proton radiography [8,9]. The combination of characteristics in our approach allow us to: first, probe distributions of self-generated  $E+B$  fields; second, determine  $\rho R$  by measuring the energy loss of backlighting protons; and third, sample all the implosion phases from acceleration, through coasting and deceleration, to final stagnation, to provide a more comprehensive picture of ICF spherical implosions. The result is the first use of proton radiography to study ICF implosion dynamics. We note that earlier work by

Mackinnon *et al.* [10] successfully demonstrated the feasibility of imaging implosions with protons (produced, in their case, by laser-plasma interactions), backlighting plastic (CH) capsules that were imploded by six 1- $\mu$ m-wavelength laser beams [11]. Most importantly as regards this paper, they did not observe any evidence of radial electric fields of the sort reported here. This is probably due to the fact that their implosions were totally different from ours [11,12].

Our experiment is illustrated schematically in Fig. 1. A CH capsule that is the imaged subject had an 860- $\mu$ m initial diameter, 20- $\mu$ m thick shell and 15-atm  $H_2$  gas fill. It was imploded through direct drive with 40 beams of frequency-tripled (0.35  $\mu$ m) UV laser light. The laser pulse was square, with a duration of 1-ns and a total energy of  $\sim 16$  kJ. Individual laser beams were smoothed using a single-color cycle, 1 THz two-dimensional (2D)

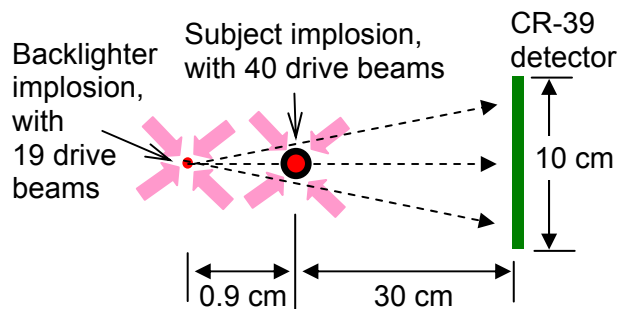


FIG. 1. (Color online) Experimental setup, with proton backlighter, subject implosion, CR-39 imaging detectors, and laser beams. The field of view at the subject is  $\sim 3$  mm.

smoothing by spectral dispersion (SSD), and polarization smoothing (PS) [13,14]. Implosions were backlit with monoenergetic protons (15.1 MeV) generated from D<sup>3</sup>He-filled, exploding-pusher implosions driven by 19 OMEGA laser beams (details of the technology have been reported elsewhere [8,9]). The backlighting duration was  $\sim 130$  ps, and the relative timing of backlighter and subject implosions was adjusted in each experiment so the proton radiograph would reflect the condition of the subject capsule at a desired time during its implosion. The effective FWHM of the backlighter is  $\approx 40 \mu\text{m}$  [8], and this is the primary limit on the intrinsic spatial resolution of the imaging system. In images of imploded capsules, spatial resolution is degraded somewhat by scattering of the imaging protons as they pass through the capsules [15,16].

Figure 2 shows a time sequence of proton radiographs covering the complete ICF implosion process from beginning through peak compression (each image from a different, but equivalent, implosion). The CR-39 detectors record the position and energy of every individual proton, so each radiograph can be displayed in two different ways: proton fluence vs. position [Fig. 2a] or mean proton energy vs. position [Fig. 2b]. In the uncompressed case (0.0 ns) the protons that passed through the shell limb lost the most energy, resulting in the dark ring of part (b), and were scattered the most, resulting in the light ring of part (a) (indicating low fluence at the detector). The images for later times provide important information about field distributions and capsule compression.

A striking feature of Fig. 2a, indicating the presence of a time-varying radial electric field, is that a strong central peak appears in the fluence images during the early stages of implosion ( $t = 0.8 - 1.4$  ns) while a strong central dip appears at later times ( $t = 1.6 - 2.1$  ns) [18]. This is

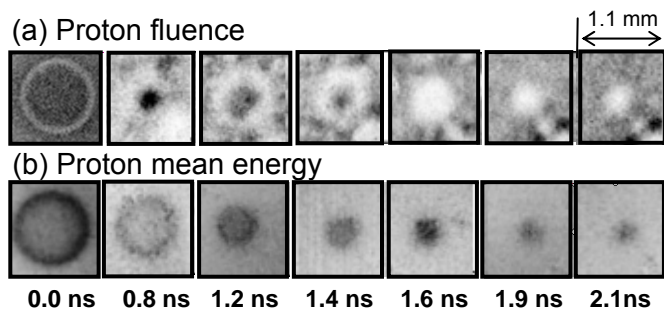


FIG. 2. 15.1-MeV proton radiographs of imploding capsules at different times, illustrating the time evolution of mass distribution and of a previously unobserved radial electric field. In the fluence images (a), darker means higher fluence, while in the energy images (b) darker means lower proton energy (more matter traversed). The gray-scale mapping is different for each image, to account for different backlighter yields (see Fig. 3) and make the most important structure clearly visible. The capsule-mounting stalk appears in the lower right corner of each fluence image, and the field of view displayed is only part of the total indicated in Fig. 1; the area outside this region is the subject of another study of external fields [17].

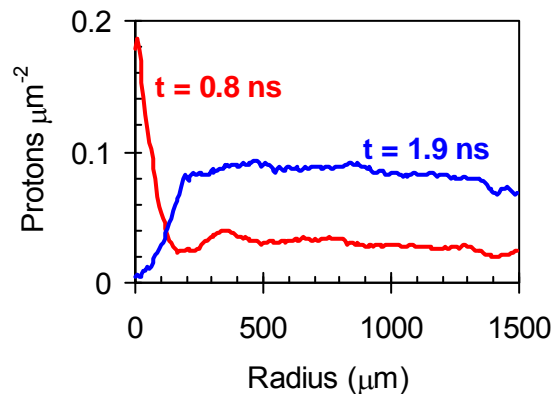


FIG. 3. (Color online) Radial profiles of two proton fluence images of Fig. 2, showing the strong central peak at  $t = 0.8$  ns and the strong central dip at 1.9 ns that can only be plausibly explained as due to radial electric fields in the capsules, not by scattering of the imaging protons. The profiles are averaged over azimuthal angle, excluding the stalk region. The difference in fluence levels outside the two capsules is due to the difference in the backlighter proton yields.

shown quantitatively in the radial lineouts of Fig. 3. As we discuss below, these features cannot be accounted for as a consequence of scatter. They must therefore result from the deflection of proton trajectories by radial electric fields. At early times the field must have been centrally directed in order to focus the protons passing within the capsule shell toward the center of the imaging detector. To account for the rapid change from a central fluence peak to a central fluence dip at  $\sim 1.5$  ns, the radial field must have either reversed direction or suddenly become at least three times larger at that time (as shown by Monte Carlo simulations), in which case all protons would strike the detector outside the shadow of the capsule (not observed).

Because of the importance of these conclusions, it is important to rule out scattering as the cause of the central peak and central dip of Fig. 3. For the earlier times, simulations show that Coulomb scattering angles are not large enough to deflect protons to the image center. For the later times, Monte Carlo simulations indicate that proton scattering can reduce the central proton fluence by  $\sim 30\%$  relative to values outside the capsule, but reductions in the actual images are  $\sim 90\%$ . In both cases, we conclude that scatter cannot be the dominant mechanism.

The  $E$ -field source that is consistent with the data is the gradient of plasma electron pressure ( $E \approx -\nabla p_e / en_e$ ) [19] (other possible sources don't fit as naturally with the data [20]). The pressure gradient has the correct sign at early times, and it reverses direction at about the correct time. This is illustrated in the  $p_e$  and  $n_e$  profiles at 0.8 ns and 1.9 ns, calculated by the LILAC hydrodynamic simulation program [21] and shown in Fig. 4. Using calculated  $\nabla p_e$  and  $n_e$  at different times, we can estimate the resultant strengths of  $E$  as varying from  $\sim -10^9$  to  $\sim 10^8$  V/m, as shown in Fig. 5. Figure 5 also shows experimental field values deduced from the data of Fig. 2a

[22]. The predictions corroborate the data in three crucial ways: the field strength and sign before the reversal ( $\sim -10^9$  V/m, directed inward), the time of the field reversal ( $\sim 1.5$  ns), and the field strength after the reversal ( $\sim 10^8$  V/m directed outward). Furthermore, Monte Carlo simulations of image formation show that only if the effects of the experimental fields are added to the effects of proton scattering can the peaks and dips of the simulations plausibly match the data [23]. This match leads to a high level of confidence that  $\nabla p_e$  is the probable source of the observed phenomena. Note that the detailed structures of the fluence images are also modified, in ways that do not affect our conclusions, by the in-flight movement of the shell ( $V_{\text{imp}} \sim -2.5 \times 10^7$  cm/s), which is  $\sim 30 \mu\text{m}$  during the backlighter burn time ( $\sim 130$  ps.)

Quantitative information about capsule sizes and  $\rho R$ s at different times is extracted from the lineouts through the centers of each of the individual images in Fig. 2b; the mean width provides the averaged capsule size ( $\approx 2R$ ), while the mean height indicates the total  $\rho L$  ( $\approx 2 \times \rho R$ ). The measurements are contrasted with LILAC simulations in Fig. 6a and 6b, respectively. The simulations come reasonably close to matching the observed evolution of capsule convergence and  $\rho R$  during the acceleration and coasting phases ( $\sim 0$ -1.6 ns), but predict somewhat smaller values of radius, and larger values of  $\rho R$ , than measured at the times of nuclear burn ( $\sim 1.9$  ns) and peak compression ( $\sim 2.1$  ns). Overall, this indicates that the implosions had approximately 1D performance, with little impact from hydrodynamic instabilities, before deceleration. It has been suggested that performance approaches 1D because

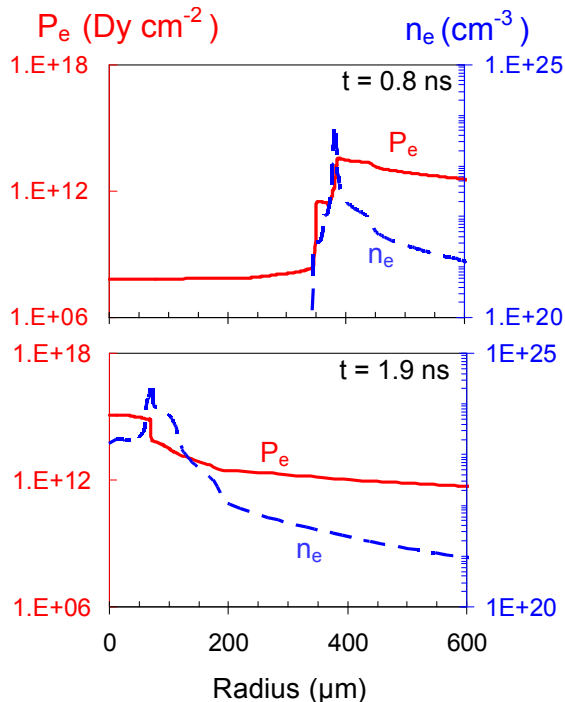


FIG. 4 (Color online) Profiles of electron pressure (solid lines) and density (dashed lines) at 0.8 ns and 1.9 ns, calculated by LILAC.

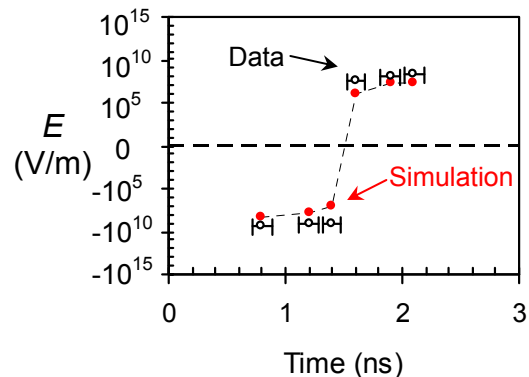


FIG. 5. (Color online) Radial  $E$  fields estimated from experimental measurements (open circles) and from LILAC simulations (solid circles) vs. implosions times. Horizontal error bars represent uncertainties in backlighter burn time. Vertical error bars are about the size of the symbols.

of full single-beam smoothing, which significantly improves the shell integrity during the acceleration phase, and because thickening of the shell during subsequent coasting further enhances shell integrity [14]. The apparent degradation of capsule performance at later times relative to the 1D simulation could be largely a consequence of fuel-shell mixing and implosion asymmetry [1].

It is worthwhile to compare these measured  $\rho R$  values with a value obtained using a completely different method

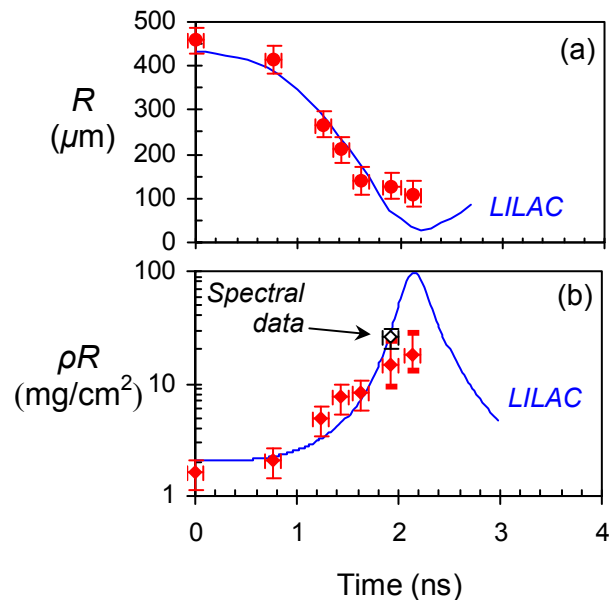


FIG. 6. (Color online) Measured capsule radii [solid circles, (a)] and  $\rho R$  [solid diamonds (b)] compared with LILAC 1D simulations (solid lines). Horizontal error bars represent uncertainties in backlighter burn time. The open diamond point in (b) represents the  $\rho R$  of a comparable implosion of a  $\text{D}^3\text{He}$ -filled capsule at bang time, measured by several proton spectrometers in different directions; this completely different type of measurement is statistically consistent with the data derived here from radiography images.

during an equivalent implosion. The open black data point in Fig. 6b was obtained by using proton spectrometry to determine the energy of self-emitted  $D^3He$  protons; the downshift in the energy of these protons implies a  $\rho R$  at bangtime of  $\sim 25$  mg/cm<sup>2</sup>. This is slightly higher than the measurement made here, but statistically consistent with it given the measurement uncertainties. On the other hand, the spectrometry-implied value is closer to the 1D value, which raises the possibility that the radiography-implied value loses accuracy when the capsule becomes sufficiently compressed that images are noticeably affected by proton scatter. This is currently being investigated, and we plan to develop a more accurate technique for deconvolving the effects of scatter in our analyses.

Finally, the residual mass during the implosion can be estimated in terms of the measured  $R$  (Fig. 6a) and measured  $\rho R$  (Fig. 6b):  $m/m_0 \approx C_r^{-2} \rho R(t)/\rho R(0)$ , where  $C_r \equiv R(0)/R(t)$  is the target convergence ratio. This indicates that  $\sim 30 - 40\%$  of the shell has been ablated by bang time. Although the mass estimates have large uncertainties due to those associated with both  $R$  and  $\rho R$  measurements, they are helpful for illustrating the dynamics of mass ablation during implosions.

In summary, new observations and measurements of direct-drive spherical implosions have been made with monoenergetic proton radiography. Quantitative information inferred from proton images characterizes the spatial structure and temporal evolution of an imploding capsule, dynamically displaying a comprehensive picture of direct-drive ICF implosions. The observations include the first experimental evidence of radial  $E$  fields inside imploding capsules, and their reversal in direction and their plausible connection with plasma pressure gradients.

The work described here was performed at the LLE National Laser User's Facility (NLUF), and was supported in part by US DOE (Grant No. DE-FG03-03SF22691), LLE (subcontract Grant No.412160-001G), LLNL (subcontract Grant No.B504974), the Fusion Science Center for Extreme States of Matter and Fast Ignition Physics at University of Rochester, and GA under DOE (DE-AC52-06NA27279).

---

[1] S. Atzeni and J. Meyer-Ter-Vehn, *The Physics of Inertial Fusion* (Clarendon Press, Oxford 2004).  
 [2] F. J. Marshall, *et al.*, Phys. Plasmas **11**, 251 (2004).  
 [3] R. S. Craxton *et al.*, Phys. Plasmas **12**, 056304 (2005).  
 [4] F. H. Séguin *et al.*, Rev. Sci. Instrum. **74**, 975 (2003).  
 [5] L. Disdier *et al.*, Phys. Plasmas **13**, 056317 (2006).  
 [6] F. H. Séguin *et al.*, Rev. Sci. Instrum. **75**, 3520 (2004).  
 [7] J. M. Soures, *et al.*, Phys. of Plasmas **3**, 2108 (1996).  
 [8] C. K. Li *et al.*, Rev. Sci. Instrum. **77**, 10E725 (2006).  
 [9] C. K. Li *et al.*, Phys. Rev. Lett. **97**, 135003 (2006).  
 [10] A. Mackinnon *et al.*, Phys. Rev. Lett. **97**,045001 (2006).

[11] In the images of Ref. [10] there is no evidence of fields in or near the capsule, in contrast to our observations here and in numerous other experiments. This difference can probably be attributed to the fact that their implosion conditions were completely different from ours. They used 6 1- $\mu$ m laser beams, without phase plates, in a 240 J, 1-ns pulse to implode a 250- $\mu$ m-radius capsule, and there were timing inconsistencies between beams [12]. We used forty 1/3- $\mu$ m, fully smoothed beams in a 16-kJ, 1-ns pulse to implode 430- $\mu$ m-radius capsules, and the beam timing was consistent to 10 ps. Their proton backlighter was also very different, with a lower energy (5-7 MeV) and broader spectrum.  
 [12] A. Mackinnon, private communication (2007).  
 [13] S. Skupsky *et al.*, Phys. Plasmas **6**, 2157 (1999).  
 [14] D. D. Meyerhofer *et al.*, Phys. Plasmas **8**, 2251 (2001).  
 [15] V. L. Highland, Nucl. Instrum. Methods **129**,497 (1975)  
 [16] A simple analytic model [14] can be used to estimate the characteristic scattering angle in radians for protons passing through a plasma with areal density  $\rho L$ :  $\langle \theta_{sc} \rangle = z (15 \text{ MeV}/p\beta c) (\rho L/\rho L_{rad})^{1/2}$ , where  $z = 1$  for protons;  $p\beta c = 30$  MeV for 15 MeV protons;  $\rho L_{rad} = 4.34 \times 10^4$  mg/cm<sup>2</sup> for carbon. For example, if  $\rho L \approx 20$  mg/cm<sup>2</sup>, then  $\langle \theta_{sc} \rangle \sim 0.6^\circ$ .  
 [17] F. H. Séguin *et al.*, paper in preparation.  
 [18] Monte Carlo simulations of the imaging system show that, for a given amount of deflection, the character of focusing or defocusing in the image is insensitive to the specific distance of the detector position.  
 [19] S. I. Braginskii, *Review of Plasma Physics* (Consultants Bureau, New York, 1965).  
 [20] For example, the contribution of charge separation around the convergent shock front due to the imbalance of ion mean-free paths between the shocked and unshocked plasmas will neither reverse direction nor suddenly increase as the data require. (We have ignored contributions from the outgoing shock front at later times due to its relatively weaker strength.)  
 [21] J. A. Delettrez *et al.*, Phys. Rev. A **36**, 3926 (1987).  
 [22] The electric field  $E$  was derived from the images by using  $E \sim 2\xi\varepsilon_p(A+a)(eAaL)^{-1}$ , where  $\varepsilon_p = 15$  MeV is the proton energy,  $e$  is electron charge,  $a = 0.9$  cm and  $A = 30.9$  cm are distances from backlighter to implosion and from backlighter to detector, respectively,  $|\xi| \sim (0.5-1) \times R$  is the apparent displacement of protons in the subject plane due to the effects of  $E$  on the proton trajectories, and  $L \sim (0.5-2) \times R$  is the proton pathlength.  
 [23] C. K. Li *et al.*, MIT PSFC Report PSFC/JA-08-3.